



Understanding magnetic behaviors of FeCoNiSi_{0.2}M_{0.2} (M=Cr, Mn) high entropy alloys via first-principle calculation

Peng Wei^a, Yanzhou Fan^a, Weiwei Zhang^a, Xuan Li^b, Shijie Zhu^a, Jianfeng Wang^a, Chao Wang^a, Tao Zhang^b, Chen Chen^{a,*}, Shaokang Guan^{a,*}

^a School of Materials Science and Engineering, Zhengzhou University, Zhengzhou 450001, China

^b Key Laboratory of Aerospace Materials and Performance (Ministry of Education), School of Materials Science and Engineering, Beihang University, Beijing 100191, China



ARTICLE INFO

Keywords:

High entropy alloy
Ferromagnetism
Density function theory
Special quasi-random structure
Magnetic properties

ABSTRACT

In this paper, first-principle calculations combining special quasi-random structure (SQS) method were utilized for detecting the mechanism of diversity in magnetic behaviors of rapid-solidified FeCoNiSi_{0.2}M_{0.2} (M=Cr, Mn) high entropy alloys (HEAs). According to the results, the crystal structure and magnetic properties calculated from the SQS structure fit well with those of the HEAs. It is found that, the addition of Mn leads to significant enhancement in saturated magnetization (B_S) and Curie temperature (T_C) of the FeCoNiSi_{0.2}M_{0.2} HEA compared to Cr, which is caused by the changes of electron-spin that lead to ferromagnetism of Mn, and such phenomenon may have close correlation with the ferromagnetic coupling between Mn and FeCoNi matrix. This work provides a novel insight for the compositional design of ferromagnetic HEAs with excellent magnetic properties.

1. Introduction

High entropy alloys (HEAs) have attracted extensive attentions due to their unique phase formation principles and excellent properties such as high strength and plasticity at high and low temperatures, outstanding hardness and corrosion resistance, etc. [1–2]. In recent years, there is a growing interest in functional properties of HEAs, especially magnetic properties, and a series of ferromagnetic HEAs systems such as Fe-Co-Ni-Al-Si, Fe-Co-Ni-Mn-Al, Fe-Co-Ni-Mn-Ga, Fe-Co-Ni-Cr-Si, Fe-Co-Ni-Mn-Si, Fe-Co-Ni-Cu-Si, etc. have been reported [3–7]. Some of them with non-equimolar ratios show good combination of soft magnetic properties and mechanical properties, such as FeCoNiCr_{0.2}Si_{0.2}, FeCoNiMn_{0.25}Al_{0.25}, etc. [8,9]. Besides, under proper processing strategies, such HEAs could also have good corrosion resistance, indicating good potential for further application in harsh environment [4]. It is noticed that, except the ferromagnetic elements, i.e., Fe, Co, Ni, the non-ferromagnetic constituent elements are also important for the magnetic properties of HEAs, especially saturated magnetization (B_S). For example, according to the report from Zhang et al. [10], the Fe-CoNiSi_{0.2}Cr_{0.2} HEA shows B_S of ~100 emu/g, while based on the results from Li et al. [11], the FeCoNiSi_{0.2}Mn_{0.2} HEA has much higher B_S of 112 emu/g. Besides, it is found that the Curie temperature (T_C) of HEAs as another significant property of magnetism is sensitive to base

composition, additional alloying elements, and crystal structure [12–13]. Moreover, non-ferromagnetic elements may have significant effects on the T_C of HEAs, for example, according to the results from Lucas et al. [14], the addition of Pd increases the T_C of FeCoCrNi HEA from below room temperature to 440 K for FeCoCrNiPd and to 503 K for FeCoCrNiPd₂. Therefore, in order to further develop HEAs with excellent magnetic properties, it is essential to understand the influences of such non-ferromagnetic elements on magnetic behaviors of these series of HEAs.

In this work, the FeCoNiSi_{0.2}M_{0.2} (M=Cr, Mn) HEAs were selected as model materials. The special quasi-random structures (SQS) is a method to produce a small crystal structure to represent the randomness of a multi-component solid-solution. This approach simulates the disordered state of a limited supercell by optimizing the atomic distribution and minimizing the correlation function, which has been proved to be effective in constructing those of HEAs [4,15], and is beneficial for further analyzing the mechanism of magnetic behaviors of the HEAs via first-principle calculation. Therefore, the crystal structures of these two alloys were decided by SQS method, and the B_S and T_C of these HEAs, as well as the density of state (DOS) of electrons in different elements were calculated. It is reported that common casting method may cause the compositional segregation and tiny precipitation formation in some HEAs, while rapid-solidification would

* Corresponding authors.

E-mail addresses: chenchennmse@zzu.edu.cn (C. Chen), skguan@zzu.edu.cn (S. Guan).

lead to the formation of homogeneous disordered solid-solution structure [3,9]. Consequently, in order to better estimate the calculation results in this work, the FeCoNiSi_{0.2}M_{0.2} (M=Cr, Mn) HEAs for the test of B_S and T_C were also produced by rapid-solidification. The mechanism for the difference between magnetic behaviors of these two HEAs are discussed in details.

2. Experimental

2.1. Computational method

In order to generate stable and reliable random high-entropy solid-solution structure of FeCoNiSi_{0.2}M_{0.2} (M=Cr, Mn), the special quasi-random structures (SQS) through the Alloy Theoretic Automated Toolkit (ATAT) package developed by Axel van de Walle et al. [16] was employed to generate a 108-atom FCC structure, and considering the composition of these HEAs, the amount of Fe, Co, and Ni atoms in this structure are 32, while those of Si and M atoms are 6. The best SQS structure was decided until its correlation mismatch parameter reached a stable value. After the best SQS structure was generated, the first-principle density functional theory (DFT) calculations based on Vienna ab initio simulation package (VASP) [17] under the generalized gradient approximation (GGA) of the Perdew-Burke-Ernzerhof (PBE) parametrization and projector-augmented wave (PAW) potential were employed to relax these structures. During optimization of the unit cell, the effect of spin polarization on the unit cell was neglected in the beginning of the process to speed up convergence, and then spin polarization was taken into account to acquire final crystal structures. Further, such structures were utilized to calculate the magnetic and electronic properties of the HEAs, which has been successfully applied to the calculation of other HEAs [18,19]. In the calculation, the k-points of $3 \times 3 \times 3$ were used to integrate the Brillouin region. The cutoff energy for the plane wave expansion was set to 400 eV. Besides, the total energies were converged to 10^{-6} eV, and the forces on each atom were relaxed to less than 0.01 eV/Å.

2.2. Experimental procedure

In terms of experiment, vacuum induction melting in high-purity argon atmosphere was used to melt the raw materials with high purity of ≥ 99.9 wt% to fabricate alloy ingots with compositions of FeCoNiSi_{0.2}M_{0.2} (M=Cr, Mn). Then ingots were re-melted under high-purity argon atmosphere and injected onto the rotating water-cooled copper wheel with the linear speed of about 32 m/s to fabricate the rapid-solidified ribbon specimens. A FEI QUANTA 200 scanning electron microscope (SEM) with energy dispersion spectrum (EDS) was employed for element mapping to estimate the chemical uniformity, and a JEM 2100 transmission electron microscope (TEM) was utilized for observation of nanoscale microstructure and identification of crystal structure in specimens. An Empyrean X-ray diffractometer (XRD) with Cu K α was applied to identify the crystal structures of these two compositions. A Lakeshore 7404 vibrating specimen magnetometer (VSM) was used for the test of hysteresis loop of the ribbon specimens and a TGA 5500 thermogravimetric analyzer (TG) with magnetic field was exploited for testing T_C of ribbon specimens.

3. Results and discussion

The back scattered images and corresponding EDS elemental mapping micrographs of the constituent elements of FeCoNiSi_{0.2}M_{0.2} (M=Cr, Mn) alloys are shown in Fig. 1(a) and (b). It could be easily found that the ribbon specimens are composed of homogeneous structure with no observable composition diversity. Fig. 1(c)~(f) exhibit bright-field image and corresponding selected area electron diffraction (SAED) patterns for these two HEAs. As shown in Fig. 1(c) and (e), cell-like grains with a size of ~ 1 μm are formed in the ribbon specimens, in

which only the chemically disordered FCC phase could be identified from the corresponding SAED patterns of FeCoNiSi_{0.2}M_{0.2} (M=Cr, Mn) shown in Fig. 1(d) and (f), respectively.

The experimental and calculated XRD patterns of FeCoNiSi_{0.2}M_{0.2} (M=Cr, Mn) are displayed in Fig. 2. It is clearly observed that, except for the FCC phase, no other phase could be found within the resolution range of XRD, indicating that both FeCoNiSi_{0.2}Cr_{0.2} and FeCoNiSi_{0.2}Mn_{0.2} alloys are composed of a completely disordered FCC structure. Moreover, the calculated XRD patterns of both FeCoNiSi_{0.2}Cr_{0.2} and FeCoNiSi_{0.2}Mn_{0.2} alloys are in line with the experimental results, indicating that the generated structures through SQS are reasonable and subsequent calculations utilizing these structures would be reliable.

The predicted magnetic moments of individual atoms in FeCoNiSi_{0.2}M_{0.2} (M=Cr, Mn) at 0 K are plotted in Fig. 3(a) and (b), respectively. For both compositions, ferromagnetic Fe, Co and Ni generally have obvious positive μ_B , while that of Si is near zero. The only difference is the role of Cr and Mn in these two components. Cr shows typical anti-ferromagnetic properties, while Mn displays strong ferromagnetism, which causes the phenomenon that total μ_B of FeCoNiSi_{0.2}Mn_{0.2} exceeds FeCoNiSi_{0.2}Cr_{0.2}. Fig. 3(c) exhibits hysteresis loops of FeCoNiSi_{0.2}M_{0.2} (M=Cr, Mn) specimens. Obviously, the present alloy in the FeCoNiSi_{0.2}Mn_{0.2} possess much higher B_S of 118.49 emu/g than that in FeCoNiSi_{0.2}Cr_{0.2} of 105.89 emu/g. The experimental B_S and calculated total magnetic moment are listed in Fig. 3(d), the units of these two could be converted to each other, of which 1 emu/g converts to an average of 1.08 μ_B /atom. Then these two compositions converted into Bohr magneton are 114.36 and 127.96 μ_B , respectively. Therefore, it could easily come to a conclusion that the calculated total magnetic moment of both HEAs show excellent consistency with the experimental B_S .

Moreover, magnetic performance under high temperature for HEAs could be measured through T_C . The experimental T_C of these two alloys are displayed in Fig. 4(a). The T_C of FeCoNiSi_{0.2}Mn_{0.2} is identified to 668 K, which is slightly higher than FeCoNiSi_{0.2}Cr_{0.2} of 656 K, indicating that these two alloys could be applied in high temperature. Here the mean-field approximation (MFA) which obtains a good approximation of the Heisenberg Hamilton equation through a method similar to Weiss molecular field theory was employed to evaluate T_C [20]. Based on MFA, T_C is directly related to the sum of magnetic interactions and obtained by calculating the energy difference between the paramagnetic (PM) and ferromagnetic (FM) states of the alloy in equilibrium through the following equation:

$$T_C = \frac{2(E_{FM} - E_{PM})}{3k_B(1 - c)} \quad (1)$$

where E_{FM} and E_{PM} are total energies per atom for the FM and PM states in equilibrium, respectively. k_B is the Boltzmann constant, and c is the concentration of the non-magnetic component.

It is found that MFA has the necessary accuracy and predictive ability, which reveals the magnetic properties of diluted magnetic semiconductors and some HEAs [20–22]. In the calculation, the total energy and exchange interaction using the DFT implemented within the framework of the accurate muffin-tin orbital (EMTO) formalism was performed. In addition, the coherent potential approximation (CPA) was employed to deal with chemical and magnetic disordered states in stochastic systems. Meanwhile, the simulation of the paramagnetic state was achieved by the disordered local moment (DLM) approximation. It is worth mentioning that all calculations were performed on completely disordered solid solutions and static lattices to ensure the calculation accuracy [21,22]. As shown in Fig. 4(b), the trend of calculated results fit well with the experimental values, and as it is well known that T_C is consistently overestimated by MFA, this result further indicates the good accuracy of the model built via SQS method. The energy of these two alloys in the PM state are similar, the difference is that the energy in the FM state Mn is slightly higher than Cr. The main reason for the difference of these studied HEAs is the appearance of the

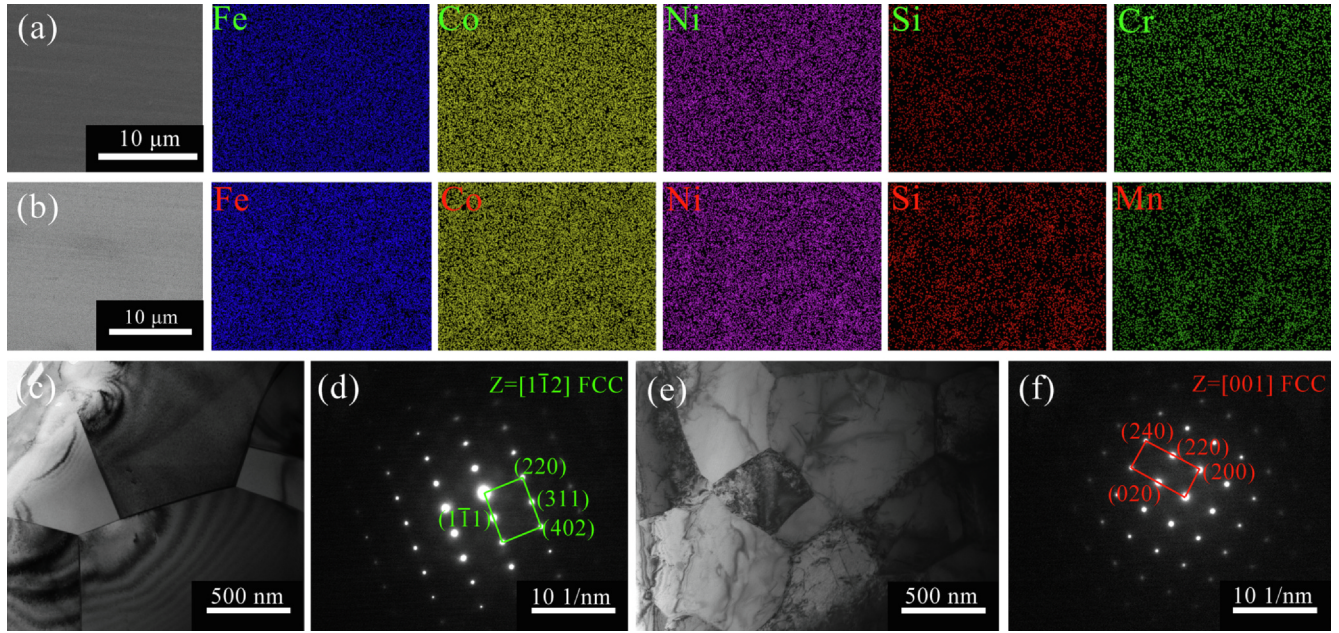


Fig. 1. (a)(b) SEM micrographs of the FeCoNiSi_{0.2}M_{0.2} (M=Cr, Mn) alloys and the distribution of the constituent elements from EDS elemental mapping in two alloys; (c) Bright-field image for the FeCoNiSi_{0.2}Cr_{0.2} alloy; (d) The corresponding SAED pattern along the[1-12] zone axis; (e) Bright-field image for the FeCoNiSi_{0.2}Mn_{0.2} alloy; (f) The corresponding SAED pattern along the[001] zone axis.

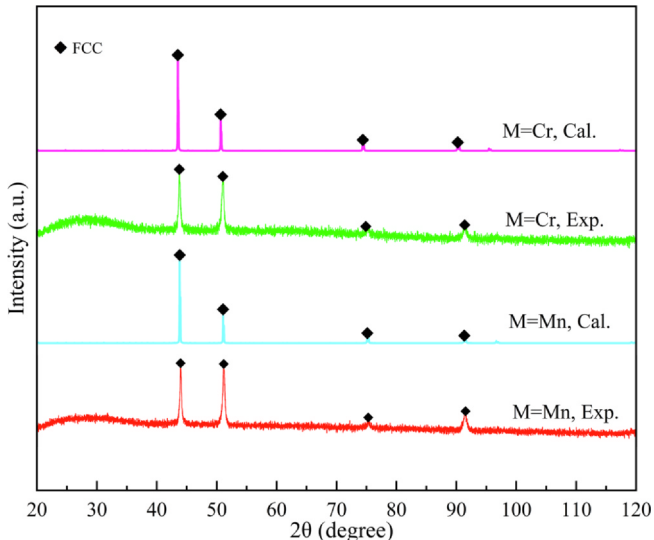


Fig. 2. The experimental and calculated XRD patterns of FeCoNiSi_{0.2}M_{0.2} (M=Cr, Mn) alloys.

ferromagnetic or anti-ferromagnetic coupling between Cr/Mn moments and the FeCoNi matrix.

In order to correlate their magnetic behaviors with electronic properties, Fig. 5(a) and (b) displays the total electron density of states (TDOS) in the vicinity of the Fermi level (E_F) for FeCoNiSi_{0.2}M_{0.2} (M=Cr, Mn) alloys. It is worth noting that E_F is set to zero. Through observing TDOS, it could be found that E_F of both compositions are located in a narrow valley, demonstrating that they are relatively stable and they show metallic properties since their TDOS at E_F is higher than zero. It is well known that the appearance of spin magnetic moment is due to the unequal occupancy of these spin-up and spin-down bands [4,23]. As shown in Fig. 5(a) and (b), the distribution of spin-up bands in both alloys is much higher than that of the spin-down. Besides, for both compositions, the spin-down distribution is very similar, while the difference is that the spin-up distribution of FeCoNiSi_{0.2}Mn_{0.2} is significantly higher than that of FeCoNiSi_{0.2}Cr_{0.2}, which results in the

diversity of total magnetic moment between these two HEAs.

The d-orbital DOS of transition metals plays a vital role in their magnetic performance of alloys. To further clarify the role of constituent elements in these studied HEAs, the partial DOS (PDOS) of Fe, Co, Ni, Cr(Mn) d-orbits are presented in Fig. 5(c)~(f) respectively. The spin-down distribution is represented by inverting the y-axis in the same figure, while the spin-up contribution is shown along the y-axis. It could be clearly seen from Fig. 5(c)~(f) that these PDOS of constituent elements are asymmetric to some extent, indicating magnetic characters and different spin polarization behaviors [4,24]. The spin-up and spin-down PDOS of Co and Ni atoms are relatively identical in these two compositions, indicating that their contribution to the magnetic properties of these studied alloys are similar. In contrary, the main diversity is the PDOS of Fe and Cr(Mn), revealing that the magnetic moment is mainly due to their different contributions. Moreover, the spin-up PDOS of Cr is far less than that of spin-down, while the PDOS of Mn is just the reverse, which could explain the phenomenon that B_S and T_C of FeCoNiSi_{0.2}Mn_{0.2} are better than FeCoNiSi_{0.2}Cr_{0.2}. Obviously, the addition of Cr and Mn also has a certain effect on the PDOS of Fe, that is, the magnetic moment of the PDOS spin-up of Fe in FeCoNiSi_{0.2}Mn_{0.2} far exceeds the spin-down, which is not the case notable in FeCoNi-Si_{0.2}Cr_{0.2}. From a theoretical perspective, both Cr and Mn exhibit anti-ferromagnetic properties. However, the addition of Mn reduces the number of down-spins, leading to the significant improvement of total magnetic moment, while the addition of Cr has no such effect in the studied HEA. Based on the above results, it could also be deduced that there may exist ferromagnetic coupling between Mn and FeCoNi matrix, while that between Cr and such matrix is anti-ferromagnetic coupling.

The magnetic properties of HEAs are sensitive to their localized distribution of electrons. Therefore, the contour plots of local electron localization function (ELF) on the (001) plane for FeCoNiSi_{0.2}M_{0.2} (M=Cr, Mn) are given in Fig. 6(a) and (b), respectively. ELF is generally applied to analyze interatomic interaction in crystal structure, ELF = 0 and 1 represent the completely delocalized state and the perfect localization, respectively [22]. The (001) plane is selected for observation because the distribution of atoms on the (001) plane could be clearly identified and the coupling between Cr(Mn) atoms and FeCoNi

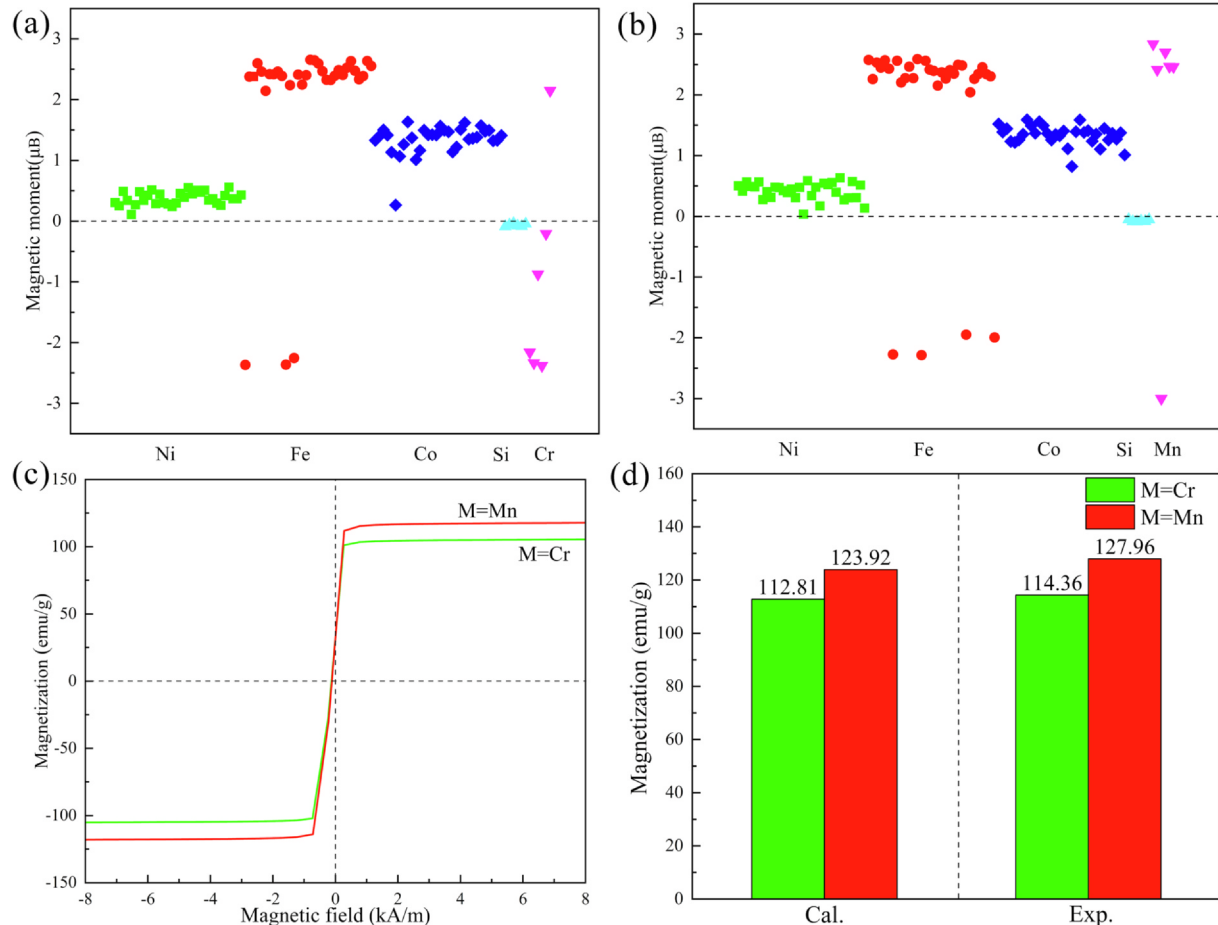


Fig. 3. (a) and (b) Magnetic moments of individual atoms of $\text{FeCoNiSi}_{0.2}\text{M}_{0.2}$ ($\text{M}=\text{Cr}, \text{Mn}$) alloys predicted from DFT calculations at 0 K; (c) Hysteresis loops of $\text{FeCoNiSi}_{0.2}\text{M}_{0.2}$ ($\text{M}=\text{Cr}, \text{Mn}$) alloys at room temperature; (d) The calculated magnetic moment and experimental B_s of $\text{FeCoNiSi}_{0.2}\text{M}_{0.2}$ ($\text{M}=\text{Cr}, \text{Mn}$) alloys.

matrix could be easily observed. As shown in Fig. 6(a) and (b), for these studied alloys, their ELF values are less than 0.5, indicating a delocalized state of electrons. Besides, there is the largest ELF value around the Mn atom, while that around Cr atom have no obvious difference with others, revealing that Mn might have a significant tendency to localize electrons nearby and further cause the strong ferromagnetic coupling between Mn and the FeCoNi matrix. The above factors may have possible correlation with the change of the magnetism of Mn atoms and excellent magnetic properties in $\text{FeCoNiSi}_{0.2}\text{Mn}_{0.2}$ HEA,

which deserves further investigations.

4. Conclusions

In conclusion, the DFT calculations were employed to understand the magnetic properties and corresponding intrinsic characteristics of the $\text{FeCoNiSi}_{0.2}\text{Cr}_{0.2}$ and $\text{FeCoNiSi}_{0.2}\text{Mn}_{0.2}$ HEAs in the atomic and electronic levels. It is noticed that, the crystal structure and magnetic properties calculated from the SQS structure fit well with experiment

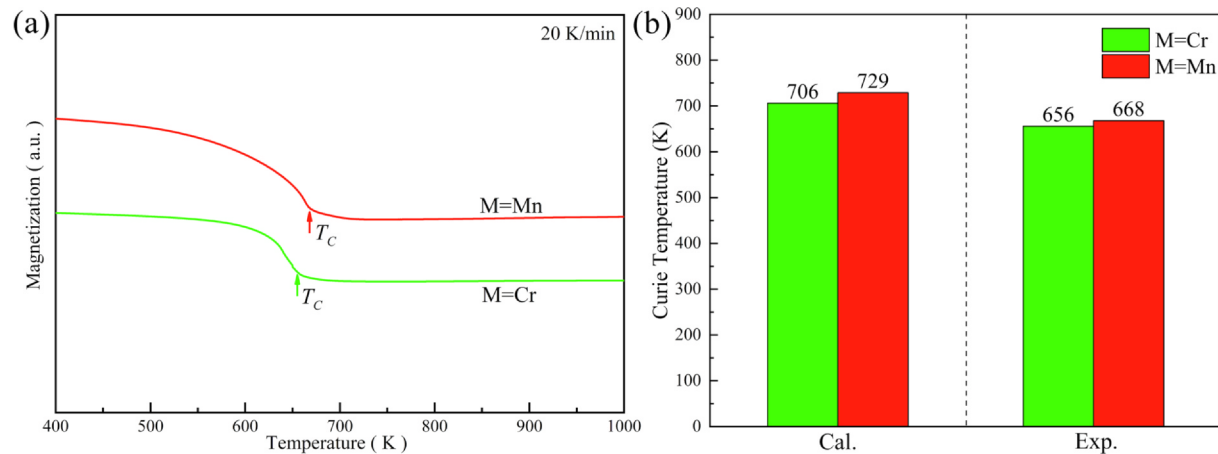


Fig. 4. (a) Curie temperature of rapid-solidified $\text{FeCoNiSi}_{0.2}\text{M}_{0.2}$ ($\text{M}=\text{Cr}, \text{Mn}$) specimens; (b) The calculated and experimental curie temperature of $\text{FeCoNiSi}_{0.2}\text{M}_{0.2}$ ($\text{M}=\text{Cr}, \text{Mn}$) alloys.

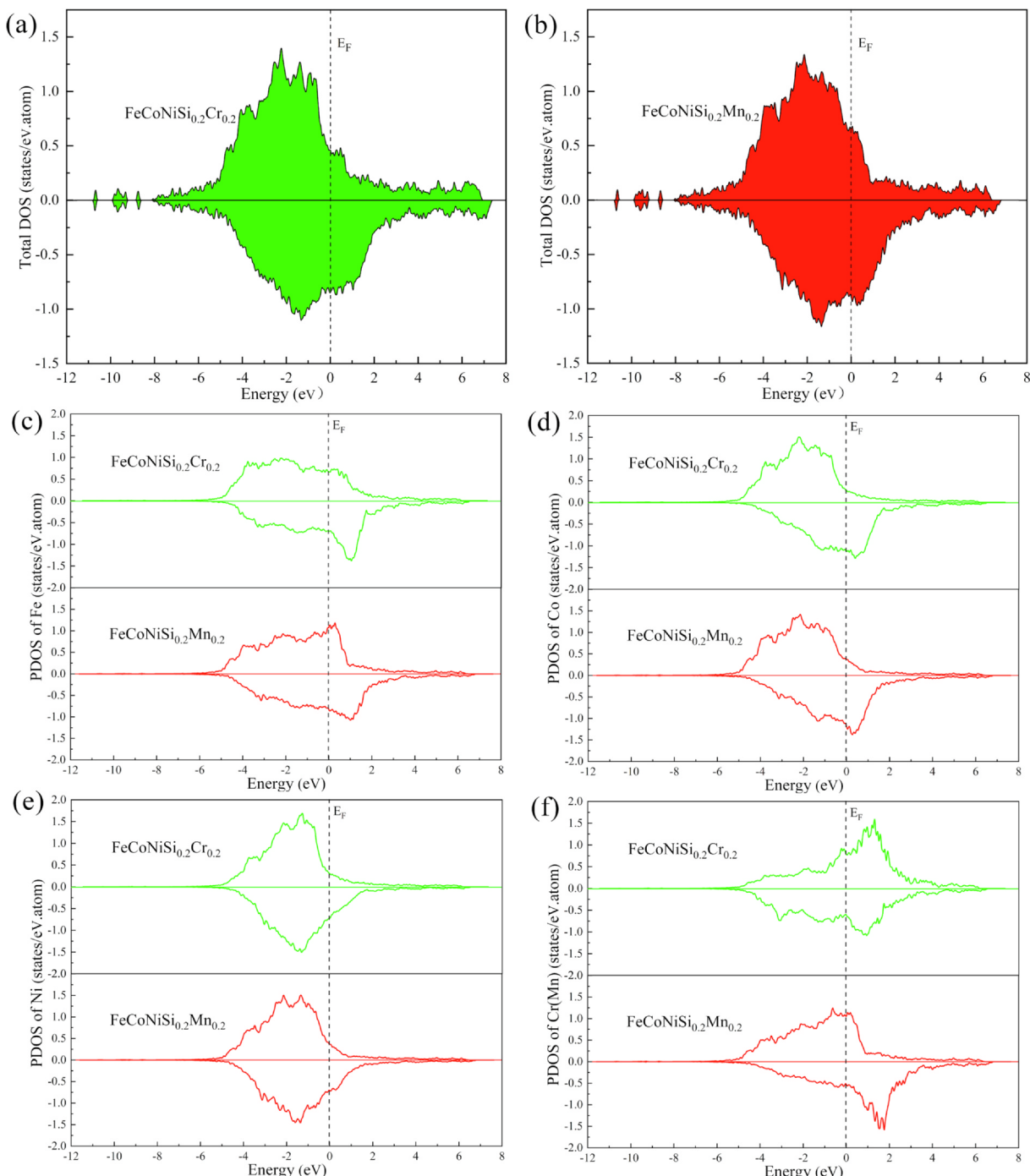


Fig. 5. (a) and (b) TDOS of $\text{FeCoNiSi}_{0.2}\text{M}_{0.2}$ ($\text{M} = \text{Cr}, \text{Mn}$) alloys; (c)~(f) the d-orbits PDOS of Fe, Co, Ni, Cr(Mn) for $\text{FeCoNiSi}_{0.2}\text{M}_{0.2}$ ($\text{M} = \text{Cr}, \text{Mn}$) alloys. The vertical dotted lines indicate in the Fermi level (E_F).

results, which can provide a reference for the composition design and optimization of HEAs. In general, the $\text{FeCoNiSi}_{0.2}\text{Mn}_{0.2}$ exhibits better ferromagnetic properties compared to $\text{FeCoNiSi}_{0.2}\text{Cr}_{0.2}$, which is manifested by the higher B_S and T_C . The doping of Mn reduces the number of spin-down electrons, leading to the transformation of Mn from the antiferromagnetic state to the ferromagnetic state, which is possibly caused by strong ferromagnetic coupling between Mn and FeCoNi matrix. This research provides a novel insight for the development of ferromagnetic HEAs.

Declaration of Competing Interest

The authors declare that they have no known competing financial interests or personal relationships that could have appeared to influence the work reported in this paper.

Acknowledgements

The work was supported by National Natural Science Foundation of China [Grant Nos. 51701183] and China Postdoctoral Science Foundation funded project [Grant Nos. 2017M622368].

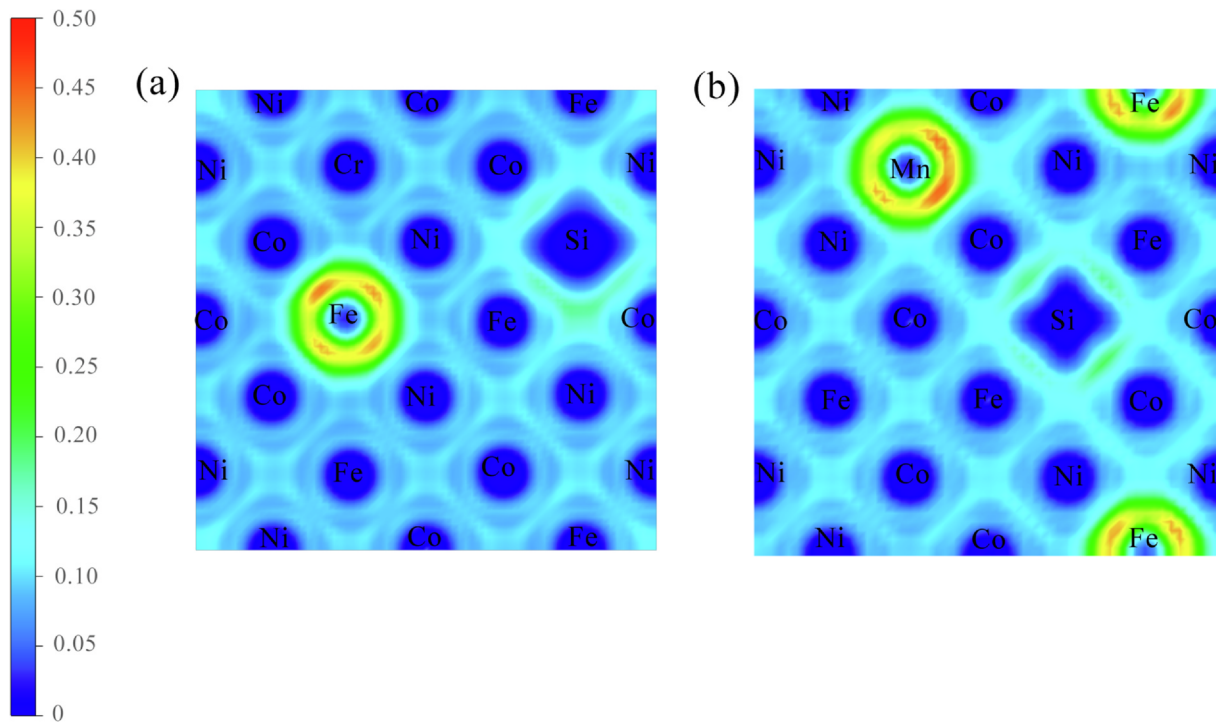


Fig. 6. (a) and (b) The contour plots of local electron localization function (ELF) for the $\text{FeCoNiSi}_{0.2}\text{M}_{0.2}$ ($\text{M}=\text{Cr}, \text{Mn}$) alloys on the (001) plane.

References

- [1] M.H. Tsai, J.W. Yeh, High-entropy alloys: a review, *Mater. Res. Lett.* 2 (3) (2014) 107–123, <https://doi.org/10.3390/met7020043>.
- [2] Y.Z. Shi, B. Yang, P.K. Liaw, Corrosion-resistant high-entropy alloys: A review, *Metals* 7 (2) (2017) 43–60, <https://doi.org/10.1080/21663831.2014.912690>.
- [3] C. Chen, H. Zhang, Y.Z. Fan, W.W. Zhang, R. Wei, T. Wang, T. Zhang, K. Wu, F.S. Li, S.K. Guan, J.Z. Jiang, Improvement of corrosion resistance and magnetic properties of $\text{FeCoNiAl}_{0.2}\text{Si}_{0.2}$ high entropy alloy via rapid-solidification, *Intermetallics* 122 (2020) 106778, <https://doi.org/10.1016/j.intermet.2020.106778>.
- [4] T.T. Zuo, Michael C. Gao, L.Z. Ouyang, X. Yang, Y. Q. Cheng, R. Feng, S.Y. Chen, Peter K. Liaw, Jeffrey A. Hawk, Y. Zhang, Tailoring magnetic behavior of CoFeMnNiX ($X=\text{Al, Cr, Ga, and Sn}$) high entropy alloys by metal doping, *Acta Mater.* 130 (2017) 10–18, <http://dx.doi.org/10.1016/j.actamat.2017.03.013>.
- [5] C. Chen, H. Zhang, S. Hu, R. Wei, T. Wang, Y. Cheng, T. Zhang, N. Shi, F. Li, S. Guan, J. Jiang, Influences of laser surface melting on microstructure, mechanical properties and corrosion resistance of dual-phase Cr–Fe–Co–Ni–Al high entropy alloys, *J. Alloys Compd.* (2020), <https://doi.org/10.1016/j.jallcom.2020.154100>.
- [6] M.C. Gao, D.B. Miracle, D. Maurice, X. Yan, Y. Zhang, J.A. Hawk, High-entropy functional materials, *J. Mater. Res.* 33 (2018) 3138–3155, <https://doi.org/10.1557/jmr.2018.323>.
- [7] H.P. Chou, Y.S. Chang, S.K. Chen, J.W. Yeh, Microstructure, thermophysical and electrical properties in $\text{Al}_x\text{CoCrFeNi}$ ($0 \leq x \leq 2$) high-entropy alloys, *Mater. Sci. Eng., B* 163 (2009) 184–189, <https://doi.org/10.1016/j.mseb.2009.05.024>.
- [8] T.T. Zuo, M. Zhang, P.K. Liaw, Y. Zhang, Novel high entropy alloys of $\text{Fe}_x\text{Co}_{1-x}\text{NiMnGa}$ with excellent soft magnetic properties, *Intermetallics* 100 (2018) 1–8, <https://doi.org/10.1016/j.intermet.2018.05.014>.
- [9] C. Chen, H. Zhang, Y.Z. Fan, W.W. Zhang, R. Wei, T. Wang, T. Zhang, F.S. Li, A novel ultrafine-grained high entropy alloy with excellent combination of mechanical and soft magnetic properties, *J. Magn. Magn. Mater.* 502 (2020) 166513, <https://doi.org/10.1016/j.jmmm.2020.166513>.
- [10] Y. Zhang, T.T. Zuo, Y. Cheng, P.K. Liaw, High-entropy alloys with high saturation magnetization, electrical resistivity, and malleability, *Sci. Rep.* 3 (2013) 1455, <https://doi.org/10.1038/srep01455>.
- [11] Z. Li, Y. Gu, M.X. Pan, C.X. Wang, Z.Y. Wu, X.L. Hou, X.H. Tan, H. Xu, Tailoring AC magnetic properties of $\text{FeCoNi}(\text{MnSi})_x$ ($0 \leq x \leq 0.4$) high-entropy alloys by the addition of Mn and Si elements, *J. Alloy. Compd.* 792 (2019) 2150925–2218388, <https://doi.org/10.1016/j.jallcom.2019.03.411>.
- [12] Y.F. Kao, S.K. Chen, T.J. Chen, P.C. Chua, J.W. Yeh, S.J. Lin, Electrical, magnetic, and Hall properties of $\text{Al}_x\text{CoCrFeNi}$ high-entropy alloys, *J. Alloy. Compd.* 509 (2011) 1607–1614, <https://doi.org/10.1016/j.jallcom.2010.10.210>.
- [13] S. Huang, Á. Vida, D. Molnár, K. Kádas, L.K. Varga, E. Holmström, L. Vitos, Phase stability and magnetic behavior of FeCrCoNiGe high-entropy alloy, *Appl. Phys. Lett.* 107 (2015) 251906, <https://doi.org/10.1063/1.4938398>.
- [14] M.S. Lucas, L. Mauger, J.A. Muñoz, Y.M. Xiao, A.O. Sheets, S.L. Semiatin, J. Horwath, Z. Turgut, Magnetic and vibrational properties of high-entropy alloys, *J. Appl. Phys.* 109 (2011) 3, <https://doi.org/10.1063/1.3538936>.
- [15] C. Niú, A.J. Zaddach, A.A. Oni, X. Sang, J.W. Hurt III, J.M. LeBeau, C.C. Koch, D.L. Irving, Spin-driven ordering of Cr in the equiatomic high entropy alloy NiFeCrCo , *Appl. Phys. Lett.* 106 (2015) 161906, <https://doi.org/10.1063/1.4918996>.
- [16] A. van de Walle, P. Tiwary, M. de Jong, D.L. Olmsted, M. Asta, A. Dick, D. Shin, Y. Wang, L.Q. Chen, Z.K. Liu, Efficient stochastic generation of special quasirandom structures, *Calphad.* 42 (2013) 13–18. <http://dx.doi.org/10.1016/j.calphad.2013.06.006>.
- [17] G. Kresse, J. Furthmüller, Efficient iterative schemes for ab initio total-energy calculations using a plane-wave basis set, *Phys. Rev. B* 54 (1996) 11169–11186, <https://doi.org/10.1103/PhysRevB.54.11169>.
- [18] N.Y. Bao, J. Zuo, Z.Y. Du, M.L. Yang, G. Jiang, L. Zhang, Computational characterization of the structural and mechanical properties of $\text{Al}_x\text{CoCrFeNiTi}_{1-x}$ high entropy alloys, *Mater. Res. Express* 6 (2019) 096519, <https://doi.org/10.1088/2053-1591/AB2877>.
- [19] X. Sun, H. Zhang, S. Lu, X. Ding, Y. Wang, L. Vitos, Phase selection rule for Al-doped CrMnFeCoNi high-entropy alloys from first-principles, *Acta Mater.* (2017), <https://doi.org/10.1016/j.actamat.2017.08.045>.
- [20] K. Sato, L. Bergqvist, J. Kudrnovský, P.H. Dederichs, O. Eriksson, I. Turek, B. Sanyal, G. Bouzerar, H. Katayama-Yoshida, V.A. Dinh, T. Fukushima, H. Kizaki, R. Zeller, First-principles theory of dilute magnetic semiconductors, *Rev. Mod. Phys.* 82 (2010) 1633–1690. <https://doi.org/10.1103/revmodphys.82.1633>.
- [21] S. Huang, E. Holmström, O. Eriksson, Mapping the magnetic transition temperatures for medium- and high-entropy alloys, L. Vitos, *Intermetallics* 95 (2018) 80–84, <https://doi.org/10.1016/j.intermet.2018.01.016>.
- [22] S. Huang, W. Li, X.Q. Li, S. Schönecker, L. Bergqvist, E. Holmström, L.K. Varga, L. Vitos, Mechanism of magnetic transition in FeCrCoNi -based high entropy alloys, *Mater. Design* (2016), <https://doi.org/10.1016/j.matdes.2016.04.053>.
- [23] Z.Q. Wen, Y.H. Zhao, J.Z. Tian, S. Wang, Q.W. Guo, H. Hou, Computation of stability, elasticity and thermodynamics in equiatomic AlCrFeNi medium-entropy alloys, *J. Mater. Sci.* 54 (2019) 2566–2576, <https://doi.org/10.1007/s10853-018-2943-7>.
- [24] S. Wang, T. Zhang, H. Hou, Y.H. Zhao, The magnetic, electronic, and thermodynamic properties of high entropy alloy CrMnFeCoNi : A first-principles study, *Phys. Status Solidi B* (2018), <https://doi.org/10.1002/pssb.201800306>.